J|A|C|S
ARTICLES
Published on Web 02/27/2002

Supramolecular Chirogenesis in Zinc Porphyrins: Equilibria, Binding Properties, and Thermodynamics

Victor V. Borovkov,*,† Juha M. Lintuluoto,† Hiromu Sugeta,† Michiya Fujiki,‡ Ryuichi Arakawa,§ and Yoshihisa Inoue*,†

Contribution from the Inoue Photochirogenesis Project, ERATO, JST, 4-6-3 Kamishinden, Toyonaka-shi, Osaka 560-0085, Japan, NTT Basic Research Laboratories, Wakamiya 3-1, Morinosato, Atsugi, Kanagawa 243-0198, Japan, and Department of Applied Chemistry, Kansai University, Suita, Osaka 564-8680, Japan

Received October 6, 2001

Abstract: Complexation mechanism, binding properties and thermodynamic parameters of supramolecular chirality induction in the achiral host molecule, *syn* (face-to-face conformation) ethane-bridged bis(zinc porphyrin), upon interaction with chiral monoamine and monoalcohol guests have been studied by means of the UV−vis, CD, ^{1}H NMR, and ESI MS techniques. It was found that the chirogenesis process includes three major equilibria steps: the first guest ligation to a zinc porphyrin subunit of the host (K_1), *syn* to *anti* conformational switching (K_S), and further ligation by a second guest molecule to the remaining ligand-free zinc porphyrin subunit (K_2), thus forming the final bis-ligated species possessing supramolecular chirality. The validity of this equilibria model is confirmed by the excellent match between the calculated and experimentally observed spectral parameters of the bis-ligated species. The second ligation proceeds in a cooperative manner as $K_2 > K_1$ for all supramolecular systems studied, regardless of the structure of the chiral ligand used. The binding properties are highly dependent on the nature of the functional group (amines are stronger binders than alcohols) and on the structure of the chiral guests (primary and aliphatic amines have overall binding constant values greater than those of secondary and aromatic amines, respectively).

Introduction

Noncovalent interactions contribute to the effective functioning of all living organisms, the major molecular building blocks of which are asymmetric compounds. Further association of these chiral molecules between each other or interaction with achiral molecules at the supramolecular level can lead to the transfer of chiral information, resulting in chirality induction in the achiral component or chirality amplification of the whole system. Thus, this phenomenon, termed supramolecular chirogenesis, plays a vital role in the metabolism of natural systems. Furthermore, this phenomenon is found in a number of important applications in the fast growing fields of nanotechnology, material science, and crystal engineering.[1] Consequently, supramolecular chirogenesis has recently attracted much multidiscipline attention in scientific community resulting in many interesting discoveries of this effect in various artificial systems.[2]

It is apparent that there are many external and internal factors affecting noncovalent interactions between the components of supramolecular systems, thus controlling the whole chirogenesis process(es). Among these factors, binding, equilibria, and thermodynamic parameters are of prime importance since they directly determine the magnitude of affinity and stability of the chiral associates. The significance of their influence on supramolecular chirogenesis has been clearly demonstrated by several extensive studies on the inclusion complexes of cyclodextrin and cyclic derivatives of resorcinol,[3] chiral guest interactions with oligomeric, tetrapyrrolic, and porphyrin hosts,[4] chiral guest−host encapsulation,[5] and DNA/RNA binding with various chromophores.[6]

Recently, we have discovered new supramolecular chirogenic systems based on the achiral bis-porphyrin host **1** (see Figure

* To whom correspondence should be addressed. E-mail: victrb@chiromor.jst.go.jp and inoue@ap.chem.eng.osaka-u.ac.jp.

† ERATO, JST.

‡ NTT Basic Research Laboratories.

§ Kansai University.

(1) (a) Bong, D. T.; Clark, T. D.; Granjia, J. R.; Ghadiri, M. R. *Angew. Chem., Int. Ed.* **2001**, *40*, 988. (b) Fenniri, H.; Mathivanan, P.; Vidale, K. L.; Sherman, D. M.; Hallenga, K.; Wood, K. V.; Stowell, J. G. *J. Am. Chem. Soc.* **2001**, *123*, 3854. (c) Song, J.; Cheng, Q.; Kopta, S.; Stevens, R. *J. Am. Chem. Soc.* **2001**, *123*, 3205. (d) Li, C. Y.; Cheng, S. Z. D.; Weng, X.; Ge, J. J.; Bai, F.; Zhang, J. Z.; Calhoun, B. H.; Harris, F. W.; Chien, L.-C.; Lotz, B. *J. Am. Chem. Soc.* **2001**, *123*, 2462. (e) Moreau, J. J. E.; Vellutini, L.; Man, M. W. C.; Bied, C. *J. Am. Chem. Soc.* **2001**, *123*, 1509. (f) Yamaguch, T.; Yamazaki, F.; Ito, T. *J. Am. Chem. Soc.* **2001**, *123*, 743. References 1g−y are in Supporting Information.

(2) (a) Ikeda, A.; Udzu, H.; Zhong, Z.; Shinkai, S.; Sakamoto, S.; Yamaguchi, K. *J. Am. Chem. Soc.* **2001**, *123*, 3872. (b) Nakashima, H.; Fujiki, M.; Koe, J. R.; Motonaga, M. *J. Am. Chem. Soc.* **2001**, *123*, 1963. (c) Schenning, A. P. H. J.; Jonkheijm, P.; Peeters, E.; Meijer, E. W. *J. Am. Chem. Soc.* **2001**, *123*, 409. (d) Terpin, A. J.; Zieglar, M.; Johnson, D. W.; Raymond, K. N. *Angew. Chem., Int. Ed.* **2001**, *40*, 157. (e) Steffen, W.; Köhler, B.; Altmann, M.; Scherf, U.; Stitzer, K.; zur Loye, H.-C.; Bunz, U. H. F. *Chem. Eur. J.* **2001**, *7*, 117. (f) Zahn, S.; Proni, G.; Spada, G. P.; Canary, J. W. *Chem. Eur. J.* **2001**, *7*, 88. References 2g−x are in Supporting Information.

(3) (a) Liu, Y.; You, C.-C.; Li, B. *Chem. Eur. J.* **2001**, *7*, 1281. (b) Liu, Y.; Li, B.; You, C.-C.; Wada, T.; Inoue, Y. *J. Org. Chem.* **2001**, *66*, 225. (c) Aoyagi, T.; Ikeda, H.; Ueno, A. *Bull. Chem. Soc. Jpn.* **2001**, *74*, 157. (d) Bortolus, P.; Marconi, G.; Monti, S.; Mayer, B.; Köhler, G.; Grabner, G. *Chem. Eur. J.* **2000**, *6*, 1578. (e) Kobayashi, K.; Asakawa, Y.; Kikuchi, Y.; Toi, H.; Aoyama, Y. *J. Am. Chem. Soc.* **1993**, *115*, 2648. (f) Kikuchi, Y.; Tanaka, Y.; Sutarto, S.; Kobayashi, K.; Toi, H.; Aoyama, Y. *J. Am. Chem. Soc.* **1992**, *114*, 10302.

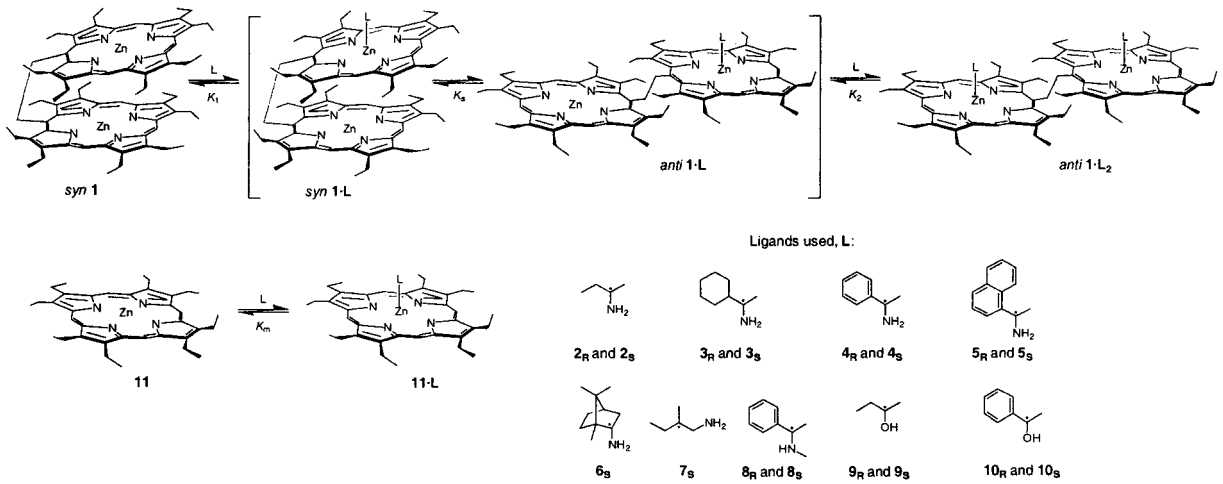

Figure 1. Structures and equilibria of the achiral dimeric and monomeric hosts (**1** and **11**, respectively) in the presence of the enantiopure amine and alcohol guests (**L**: **2**−**10**). The subscript ($_R$ or $_S$) indicates the absolute configuration of the asymmetric carbon (marked by an asterisk) which is closest to the amine binding group.

1), which undergoes structural deformations upon interactions with chiral amine and alcohol guests.[7] Spectral properties of the resulting ligand-bound complexes differ drastically from those of the nonbound host, allowing its use as an effective sensor for molecular recognition. Particularly, the most intriguing property of these systems is chirality induction in achiral host **1** which can be easily detected by CD spectroscopy. The mechanism and various internal and external factors that influence the chirogenesis process in **1** have been thoroughly investigated.[7] It was shown that the process of supramolecular chirogenesis in **1** is highly sensitive to the structure of chiral guests, with dependencies on the guest's absolute configuration, nature of the binding group, bulkiness of substituents at the chiral center, position of the binding site relative to the asymmetric carbon, and temperature. However, the host−guest affinity and complexation mechanism have yet to be analyzed in detail.

We report here systematic studies of the detailed equilibria of **1** upon interaction with chiral amine and alcohol guests and roles of the binding and thermodynamic properties in supramolecular chirogenesis, as investigated by UV−vis, CD, ^{1}H NMR, and ESI MS spectral techniques.

Experimental Section

Materials. The *syn* conformer of host **1** in which the two porphyrin planes are fixed in a face-to-face orientation (see Figure 1) was synthesized according to previously reported methods.[8] Chiral amines **2**−**8**, chiral alcohols **9**−**10**, and (octaethylporphyrinato)zinc (**11**) shown in Figure 1, anhydrous CH_2Cl_2 for UV−vis and CD measurements, and $CDCl_3$ for ^{1}H NMR and ESI MS studies were purchased from Fluka Chemica AG and Aldrich Chemical Co. and used as received.

Spectroscopic Measurements. Room temperature UV and CD spectra were measured on a Shimadzu UV-3101PC spectrometer and JASCO J-720 spectropolarimeter, respectively. Scanning conditions were as follows: scanning rate = 50 nm per min, bandwidth = 1 nm, response time = 0.5 s, accumulations = 1 scan. Various-temperature (VT) UV and CD spectra were measured simultaneously on a JASCO J-720 spectropolarimeter equipped with a liquid nitrogen-controlled quartz cell (path length = 5 mm) in a cryostat, at temperatures ranging from 296 to 169 K. Scanning conditions were as follows: scanning rate = 100 nm per min, bandwidth = 2 nm, response time = 0.5 s. The solution temperature in the cryostat was monitored directly by immersing a thermocouple into the solution.

^{1}H NMR spectra were recorded at 400 MHz on a JEOL JNM-EX 400 spectrometer. Chemical shifts were referenced to the residual proton resonance in $CDCl_3$ (δ 7.25 ppm).

The porphyrin and amine (in the case of VT measurements) concentrations used for the UV−vis, CD, ^{1}H NMR measurements are listed in the footnotes of the corresponding tables. The concentrations of chiral ligands for the VT experiments were set to ensure that the resulting mixture is CD silent at room temperature, which corresponds to more than 80% of **1** being in the *syn* conformation.

ESI MS spectra were measured on a FINNIGAN MAT TSQ 700 spectrometer. The sample solutions at room temperature were infused directly into the mass spectrometer at a rate of 3 mL/min with the spray voltage of 4.5 kV. The resulting small particles were introduced into a heated capillary for desolvation, the temperature of which was varied from 343 to 383 K.

Titration Experiments. The UV−vis and CD titration experiments were carried out as follows. Portions of a solution of chiral amine in CH_2Cl_2 were added to the solution of **1** or **11** (3 mL) in CH_2Cl_2 (for concentrations of porphyrins, see Table 1 for **11** and Table 2 for **1**) in a quartz cell, and UV−vis and CD spectra were taken after each addition. The obtained spectra were corrected for the decrease in the bis(Zn porphyrin) concentration.

^{1}H NMR titration experiments were done as follows. Portions of a solution of chiral amine in $CDCl_3$ were added to the solution of **1** (600 μL) in $CDCl_3$ (for concentrations of **1**, see Table 4) in a 5 mm o.d.

(4) (a) Tanatani, A.; Mio, M. J.; Moore, J. S. *J. Am. Chem. Soc.* **2001**, *123*, 1792. (b) Prince, R. B.; Barnes, S. A.; Moore, J. S. *J. Am. Chem. Soc.* **2000**, *122*, 2758. (c) Mizutani, T.; Sakai, N.; Yagi, S.; Takagishi, T.; Kitagawa, S.; Ogoshi, H. *J. Am. Chem. Soc.* **2000**, *122*, 748. (d) Mizutani, T.; Yagi, S.; Honmaru, A.; Murakami, S.; Furusyo, M.; Takagishi, T.; Ogoshi, H. *J. Org. Chem.* **1998**, *63*, 8769. (e) Král, V.; Rusin, O.; Schmidtchen, F. P. *Org. Lett.* **2001**, *3*, 873. (f) Sugasaki, A.; Ikeda, M.; Takeuchi, M.; Shinkai, S. *Angew. Chem., Int. Ed.* **2000**, *39*, 3839. References 4g−p are in Supporting Information.

(5) Rivera, J. M.; Martín, T.; Rebek, J., Jr. *Science* **2000**, *289*, 606.

(6) (a) Becker, H.-C.; Nordén, B. *J. Am. Chem. Soc.* **1997**, *119*, 5798. (b) Uno, T.; Hamasaki, K.; Tanigawa, M.; Shimabayashi, S. *Inorg. Chem.* **1997**, *36*, 1676. (c) Tjahjono, D. H.; Akutsu, T.; Yoshioka, N.; Inoue, H. *Biochim. Biophys. Acta* **1999**, 1.

(7) (a) Borovkov, V. V.; Lintuluoto, J. M.; Inoue, Y. *J. Am. Chem. Soc.* **2001**, *123*, 2979. (b) Borovkov, V. V.; Yamamoto, N.; Lintuluoto, J. M.; Tanaka, T.; Inoue, Y. *Chirality* **2001**, *13*, 329. (c) Borovkov, V. V.; Lintuluoto, J. M.; Fujiki, M.; Inoue, Y. *J. Am. Chem. Soc.* **2000**, *122*, 4403. (d) Borovkov, V. V.; Lintuluoto, J. M.; Inoue, Y. *Org. Lett.* **2000**, *2*, 1565. (e) Borovkov, V. V.; Lintuluoto, J. M.; Inoue, Y. *J. Phys. Chem. A* **2000**, *104*, 9213.

(8) (a) Borovkov, V. V.; Lintuluoto, J. M.; Inoue, Y. *Synlett* **1998**, 768. (b) Borovkov, V. V.; Lintuluoto, J. M.; Inoue, Y. *Helv. Chim. Acta* **1999**, *82*, 919.

NMR tube and ^{1}H NMR spectra were taken after each addition. The monitored $\Delta\delta$ values were corrected for the increase in the total amine concentration.

Definition of the Binding Parameters for Monomeric 11 Complexation. The association constants (K_m) and molar absorption coefficients (ϵ_{calc}) for the 1:1 chiral amine−monomeric **11** complexation model

$$\mathbf{11} + \mathbf{L} \rightleftarrows \mathbf{11}\cdot\mathbf{L} \quad (1)$$

were obtained as the optimized parameters from the nonlinear least-squares curve fitting of the UV−vis complexation-induced optical density changes at 293 K to the theoretical equations. For the equilibrium 1, the following equations were taken into consideration:

$$K_m = [\mathbf{11}\cdot\mathbf{L}]/([\mathbf{11}][\mathbf{L}])$$

$$\Delta P_{obs} = \Delta P_{calc}[\mathbf{11}\cdot\mathbf{L}]/([\mathbf{11}\cdot\mathbf{L}]+[\mathbf{11}])$$

$$\Delta P_{obs} = P_{obs} - P_0 \quad \Delta P_{calc} = P_{calc} - P_0$$

where P_{obs}, P_0, and P_{calc} are the observed, initial, and calculated optical densities at the maximum of the corresponding B transition wavelength of **11**·**L**, respectively. Then the ϵ_{calc} values were obtained from P_{calc} at known concentrations of **11**.

Definition of the Binding Parameters for the Bis-porphyrin 1 Complexation (Method A). The association constants (K_1', K_1, K_S, K_2), molar absorption coefficients (ϵ_{calc}), CD amplitudes (A_{calc}), and chemical shifts (δ_{calc}) were obtained as the optimized parameters by the nonlinear least-squares curve fitting of the UV−vis, CD, and ^{1}H NMR complexation-induced optical density, CD intensity, and chemical shift changes, correspondingly, at 293 K to the theoretical equations as follows.

First, the simpler two-step complexation model was considered from the following equilibria:

$$\textit{syn}\text{-}\mathbf{1} + \mathbf{L} \rightleftarrows \textit{anti}\text{-}\mathbf{1}\cdot\mathbf{L} \quad (2)$$

$$\textit{anti}\text{-}\mathbf{1}\cdot\mathbf{L} + \mathbf{L} \rightleftarrows \textit{anti}\text{-}\mathbf{1}\cdot\mathbf{L}_2 \quad (3)$$

For obtaining K_1', K_2, and the corresponding spectral parameters, the following equations were taken into consideration:

$$K_1' = [\textit{anti}\text{-}\mathbf{1}\cdot\mathbf{L}]/([\textit{syn}\text{-}\mathbf{1}][\mathbf{L}])$$

$$K_2 = [\textit{anti}\text{-}\mathbf{1}\cdot\mathbf{L}_2]/([\textit{anti}\text{-}\mathbf{1}\cdot\mathbf{L}][\mathbf{L}])$$

$$\Delta P_{obs} = C_{por}(\Delta P_{1calc}'K_1'[\mathbf{L}] + \Delta P_{2calc}K_1'K_2[\mathbf{L}]^2)/(1 + K_1'[\mathbf{L}] + K_1'K_2[\mathbf{L}]^2)$$

$$\Delta P_{obs} = P_{obs} - P_0 \quad \Delta P_{1calc}' = P_{1calc}' - P_0 \quad \Delta P_{2calc} = P_{2calc} - P_0$$

$$C_{por} = [\textit{syn}\text{-}\mathbf{1}] + [\textit{anti}\text{-}\mathbf{1}\cdot\mathbf{L}] + [\textit{anti}\text{-}\mathbf{1}\cdot\mathbf{L}_2]$$

$$[\mathbf{L}] = C_{lig} - C_{por}(K_1'[\mathbf{L}] + 2K_1'K_2[\mathbf{L}]^2)/(1 + K_1'[\mathbf{L}] + K_1'K_2[\mathbf{L}]^2)$$

$$C_{lig} = [\mathbf{L}] + [\textit{anti}\text{-}\mathbf{1}\cdot\mathbf{L}] + 2[\textit{anti}\text{-}\mathbf{1}\cdot\mathbf{L}_2]$$

where P_{obs}, P_0, P_{1calc}', and P_{2calc} are the observed, initial, and calculated spectral parameters which are optical densities at the maximum of the corresponding $B_{||}$ transition wavelength, CD amplitudes, and chemical shifts for the most downfield shifted 10,20-*meso* proton of *anti*-**1**·**L** (in the case of P_{1calc}') and *anti*-**1**·$\mathbf{L}_2$ (in the case of P_{2calc}).

Second, equilibrium 2 was divided into two equilibria.

$$\textit{syn}\text{-}\mathbf{1} + \mathbf{L} \rightleftarrows \textit{syn}\text{-}\mathbf{1}\cdot\mathbf{L} \quad (4)$$

$$\textit{syn}\text{-}\mathbf{1}\cdot\mathbf{L} \rightleftarrows \textit{anti}\text{-}\mathbf{1}\cdot\mathbf{L} \quad (5)$$

Using the defined K_1', K_2, and P_{2calc} values as described above, the K_1, K_S, and corresponding spectral parameters were obtained from the optimization of the following equations:

$$K_1 = [\textit{syn}\text{-}\mathbf{1}\cdot\mathbf{L}]/([\textit{syn}\text{-}\mathbf{1}][\mathbf{L}])$$

$$K_S = [\textit{anti}\text{-}\mathbf{1}\cdot\mathbf{L}]/[\textit{syn}\text{-}\mathbf{1}\cdot\mathbf{L}]$$

$$K_1' = K_1K_S$$

$$\Delta P_{obs} = C_{por}(\Delta P_{1calc}K_1[\mathbf{L}] + \Delta P_{Scalc}K_1K_S[\mathbf{L}] + \Delta P_{2calc}K_1K_SK_2[\mathbf{L}]^2)/(1 + K_1[\mathbf{L}] + K_1K_S[\mathbf{L}] + K_1K_SK_2[\mathbf{L}]^2)$$

$$\Delta P_{obs} = P_{obs} - P_0 \quad \Delta P_{1calc} = P_{1calc} - P_0$$

$$\Delta P_{Scalc} = P_{Scalc} - P_0 \quad \Delta P_{2calc} = P_{2calc} - P_0$$

$$C_{por} = [\textit{syn}\text{-}\mathbf{1}] + [\textit{syn}\text{-}\mathbf{1}\cdot\mathbf{L}] + [\textit{anti}\text{-}\mathbf{1}\cdot\mathbf{L}] + [\textit{anti}\text{-}\mathbf{1}\cdot\mathbf{L}_2]$$

$$[\mathbf{L}] = C_{lig} - C_{por}(K_1[\mathbf{L}] + K_1K_S[\mathbf{L}] + 2K_1K_SK_2[\mathbf{L}]^2)/(1 + K_1[\mathbf{L}] + K_1K_S[\mathbf{L}] + K_1K_SK_2[\mathbf{L}]^2)$$

$$C_{lig} = [\mathbf{L}] + [\textit{syn}\text{-}\mathbf{1}\cdot\mathbf{L}] + [\textit{anti}\text{-}\mathbf{1}\cdot\mathbf{L}] + 2[\textit{anti}\text{-}\mathbf{1}\cdot\mathbf{L}_2]$$

where P_{1calc} and P_{Scalc} are the calculated optical densities at the maximum of the corresponding $B_{||}$ transition wavelength, CD amplitudes, and chemical shifts for the most downfield shifted 10,20-*meso* proton of *syn*-**1**·**L** (in the case of P_{1calc}) and *anti*-**1**·**L** (in the case of P_{Scalc}). Then the ϵ_{calc} and A_{calc} values were obtained from P_{calc} at the known concentrations of **1**.

Definition of the Binding Parameters and Spectral Profiles for the Bis-porphyrin 1 Complexation (Method B). Probable complexation equilibria models were analyzed, and the association constants (K_1', K_1'', and K_2) for the corresponding equilibria models and calculated UV−vis and CD spectral profiles were obtained by the nonlinear least-squares method developed for a multicomponent equilibrium system and monitored over a wide wavelength range.[9] In general, the observed UV−vis or CD absorbance (D_λ) at the wavelength (λ) was expressed by the sum of absorption of the equilibrium components (i) as

$$D_\lambda = \sum \epsilon_{\lambda i}C_i(K)$$

where $\epsilon_{\lambda i}$ is the molar absorption coefficient of the i component, and $C_i(K)$ is the equilibrium concentration of the i component, which is a function of a set of the association constants K. The regions of 340−460 nm and 390−460 nm for the analysis of the UV−vis and CD spectral data, respectively, were used for calculation of the K and $\epsilon_{\lambda i}$ values at every 2 nm. Altogether for method B, the following three equilibria models were examined (in all case starting from *syn*-**1**): *model 1*, defined as K_1' by equilibrium 2 which is 1:1 complexation forming only *anti*-**1**·**L**; *model 2*, defined as K_1'' which is simultaneous 1:2 complexation according to the equilibrium

$$\textit{syn}\text{-}\mathbf{1} + \mathbf{2L} \rightleftarrows \textit{anti}\text{-}\mathbf{1}\cdot\mathbf{L}_2 \quad (6)$$

with $K_1'' = [\textit{anti}\text{-}\mathbf{1}\cdot\mathbf{L}_2]/([\textit{syn}\text{-}\mathbf{1}][\mathbf{L}]^2)$; *model 3*, defined by K_1' and K_2 which is stepwise 1:2 complexation according to the equilibria 2 and 3.

Definition of the Thermodynamic Parameters, $\Delta H°$ and $\Delta S°$, Using a van't Hoff-Type Analysis. The association constants (K) for the ligation-induced spectral changes at each temperature according to the total equilibrium 6 were obtained from the corresponding equation

(9) Sugeta, H. *Bull. Chem. Soc. Jpn.* **1981**, *54*, 3706.

at constant concentration conditions. $\Delta H°$ and $\Delta S°$ were then obtained from the following equation:

$$P_{obs} = (1-\alpha)P_0 + \alpha P_{2calc}$$

where P_{obs}, P_0, and P_{2calc} are spectral parameters as defined above and α is the molar fraction of *anti*-**1**·$\mathbf{L}_2$ ($\alpha = [anti\text{-}\mathbf{1}\cdot\mathbf{L}_2]/([syn\text{-}\mathbf{1}] + [anti\text{-}\mathbf{1}\cdot\mathbf{L}_2]$).

Since $K = e^{-\Delta H°/RT}\, e^{\Delta S°/R}$, $P_{obs} = \{1 - [Z/(Z + 1)]\}P_0 + [Z/(Z + 1)]P_{2calc}$ where $Z = e^{-\Delta H°/RT}\, e^{\Delta S°/R}\, [\mathbf{L}]^2$. P_{obs} is thus represented as a function that contains T as an independent variable and P_0, P_{2calc}, $\Delta H°$, and $\Delta S°$ as optimized parameters for the nonlinear least-squares fitting procedure.

Results and Discussion

1. Supramolecular Systems. Recently we have found that bis-porphyrin **1**[8] which is connected by a short covalent ethane bridge (Figure 1) is a host molecule well-suited for studying the processes of supramolecular chirality induction.[7] This compound exists in a *syn* conformation (*syn*-**1**) in nonpolar ligand-free solvents due to strong intermolecular $\pi-\pi$ interactions between the two zinc porphyrin macrocycles, with external ligation leading to conformational switching and formation of the *anti* form (*anti*-**1**·$\mathbf{L}_2$).[10,11] The spectral properties of *syn*-**1** and *anti*-**1**·$\mathbf{L}_2$ are very distinct, allowing the facile differentiation of the nonbound and ligated species. In the presence of chiral ligands, besides *syn*−*anti* conformational changes, there is another process of structural deformation in **1** resulting in the generation of a chiral screw structure via a steric repulsion mechanism, and hence transformation of the point chirality of the guest molecules into supramolecular chirality of the whole system. The chirogenesis induction mechanism and influence of the various external and internal factors on this process have been thoroughly studied.[7] Briefly, the chirogenesis mechanism is based on the two ligands' approach from the same side of bis(Zn porphyrin) to each zinc porphyrin subunit resulting in chiral steric repulsion between the bulkiest substituent on the asymmetric carbon of the chiral ligand and the ethyl group at either the 3- or 7-position of the neighboring porphyrin ring (depending on the absolute configuration of the ligand), and thus leading to the formation of the screw structure. For example, it was shown that (*S*)-ligands yield the right-handed screw, while (*R*)-ligands give the left-handed screw that correspond to the positive and negative chirality, respectively. This is true for the cases when the order of the substituents' bulkiness at the asymmetric carbon coincides with the priority rule according to the Cahn−Ingold−Prelog system for absolute configuration assignment, while in the cases of the inverse order the chirality sign becomes opposite.

Amines have been chosen as chiral guests because of their well-known ability to coordinate to zinc porphyrins and form stable pentacoordinate adducts at room temperature.[12] To investigate the detailed equilibria, binding, and thermodynamic parameters of supramolecular chirality induction in **1**, various commercially available amines **2**−**8** and alcohols **9** and **10** of the same structures as used in previous studies[7a,c−e] and shown in Figure 1 have been selected as external ligands in this study to investigate the chirogenesis process comprehensively.

However, since the achiral host **1** consists of two porphyrin macrocycles the binding of two ligands to each of the zinc porphyrin subunits may occur in an independent or cooperative manner. Therefore, to elucidate the contribution of each single zinc porphyrin subunit to the total equilibria process and to obtain the corresponding binding parameters, interactions of the monomeric host **11** with several chiral amines have been investigated.

2. Guest Binding to the Monomeric Host 11 as Determined by the UV−Vis Spectroscopy. The complexation behaviors of the monomeric host **11** and various chiral amines **2**−**5** were examined, and corresponding binding parameters were obtained by UV−vis spectroscopic titration experiments. However, CD spectroscopy could not be effectively applied due to the weak induced CD signals in **11**.[7a]

Stepwise addition of **2**−**5** to **11** results in pronounced UV−vis spectral changes which finally correspond to those observed in the cases of the amine-saturated conditions[7a] and are independent of the guest's structure. A typical example is shown in Figure 2. Thus, the intensities of the Soret band (corresponding to the porphyrin B transition) and visible bands (corresponding to the porphyrin Q transitions) of the ligand-free **11** gradually decrease upon increase of the ligand concentration, and new bathochromically shifted (by 11−14 nm) B- and Q-bands and a high-energy transition band at 336 nm appear, forming five clear isosbestic points. These spectral changes are associated with the amine coordination on the zinc porphyrin and consequent p_z-a_{2u} ligand−porphyrin orbital mixing. This effect is well-known and has been reported for various monomeric zinc porphyrins.[12,13]

The UV−vis changes are followed at the wavelength corresponding to the maximum of the red-shifted B transition and plotted versus the ligand molar excess, exhibiting a clear saturation behavior (Figure 3). The experimental points fit well to a set of theoretical equations for the simple 1:1 complexation isotherm using the nonlinear least-squares optimization (see equilibrium 1 in the Experimental Section), agreeing well with the pentacoordinate complexation characteristics of zinc porphyrins as mentioned above. We have used these equations to obtain the ϵ_{calc}, K_m, and the Gibbs free energy change ($\Delta G°$) values which are listed in Table 1. Calculated molar absorption coefficients are generally in good agreement with the experimentally observed coefficients (ϵ_{exp}) at saturated amine concentration conditions.[7a] As expected, the binding constants are essentially the same for the (*R*)- and (*S*)-enantiomers of the corresponding guest, within experimental error, and are strongly dependent upon the ligand structure, varying from 1800 to 7800 M^{-1}. Such values are common and within the same range of magnitude for amine binding to other monomeric zinc porphyrins.[14] The guest affinity toward zinc porphyrins is directly dependent on the ligand basicity.[13a] Reflecting this tendency, the aliphatic amines show stronger binding abilities in comparison to the benzylic amines, whose pK_a values are smaller.[15]

(10) (a) Borovkov, V. V.; Lintuluoto, J. M.; Inoue, Y. *Tetrahedron Lett.* **1999**, *40*, 5051. (b) Borovkov, V. V.; Lintuluoto, J. M.; Inoue, Y. *J. Phys. Chem. B* **1999**, *103*, 5151.

(11) Detailed mechanism and energetics of the destruction of the intramolecular $\pi-\pi$ interactions between two zinc porphyrin subunits in **1** upon binding of an external ligand based on ab initio calculations will be reported elsewhere: Lintuluoto, J. M.; Lintuluoto, M.; Borovkov, V. V.; Inoue, Y. Manuscript in preparation.

(12) Smith, K. M. *Porphyrins and Metalloporphyrins*; Elsevier: Amsterdam, 1975.

(13) (a) Kirksey, C. H.; Hambright, P.; Storm, C. B. *Inorg. Chem.* **1969**, *8*, 2141. (b) Miller, J. R.; Dorough, G. D. *J. Am. Chem. Soc.* **1952**, *74*, 3977.

(14) Izatt, R. M.; Bradshaw, J. S.; Pawlak, K.; Bruening, R. L.; Tarbet, B. J. *Chem. Rev.* **1992**, *92*, 1261.

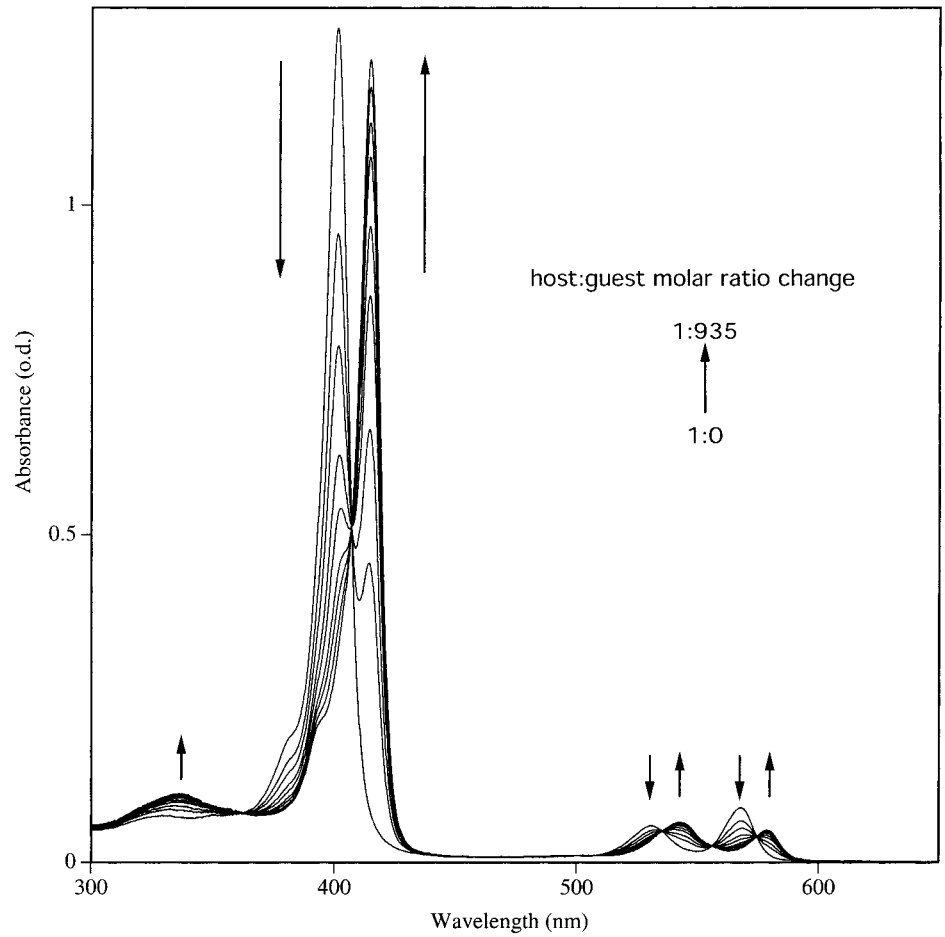

Figure 2. UV−vis spectral changes of **11** ($C = 3.2 \times 10^{-6}$ M) in CH_2Cl_2 upon addition of $\mathbf{3_R}$ as the host:guest molar ratio changes from 1:0 to 1:935.

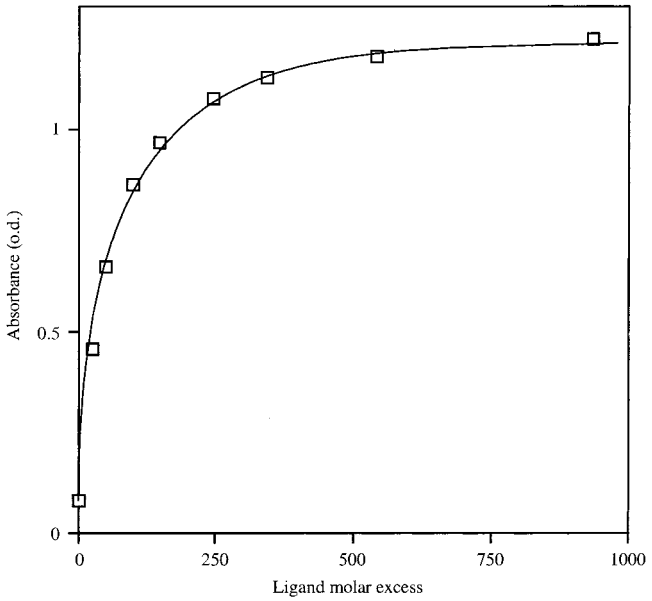

Figure 3. Dependence of the UV−vis absorbance of **11** (monitored at 415 nm) upon the molar excess of $\mathbf{3_R}$.The solid line represents the best theoretical fit for the 1:1 host−guest complexation process (see Experimental Section).

However, there are some additional factors contributing to the complexation behavior. For example, the expanded aromatic system of **5** apparently causes stronger $\pi-\pi$ interactions with

(15) Fasman, G. D. *Handbook of Biochemistry and Molecular Biology.* 3rd ed; Physical and Chemical Data. Volume I; CRC Press: Cleveland, 1975.

Table 1. Binding and UV−Vis Spectral Data of the System **11·L** with Different Chiral Amines[a]

system	binding constant K_m[b] (M^{-1})	Gibbs free energy $\Delta G°$ at 293 K[c] (kcal mol^{-1})	calculated UV–vis data ϵ_{calc}[d] (10^5 ($M^{-1}cm^{-1}$)) [λ_{max} (nm)]	observed UV–vis data ϵ_{exp}[e] (10^5 ($M^{-1}cm^{-1}$)) [λ_{max} (nm)]
11·2$_R$	3200	−4.7	3.55 [414]	4.01 [414]
11·2$_S$	3500	−4.8	3.88 [414]	3.88 [414]
11·3$_R$	7800	−5.2	3.70 [415]	3.93 [415]
11·3$_S$	7700	−5.2	3.61 [415]	3.80 [415]
11·4$_R$	2000	−4.4	3.49 [414]	3.80 [414]
11·4$_S$	1800	−4.4	3.55 [414]	3.77 [414]
11·5$_R$	3700	−4.8	3.61 [414]	3.75 [414]
11·5$_S$	3700	−4.8	3.65 [414]	3.79 [414]

[a] $C_{\mathbf{11}} = (3.0-3.3) \times 10^{-6}$ M in CH_2Cl_2. [b] The standard deviations are less than 5%. [c] $\Delta G° = -RT \ln(K_m)$, where $T = 293$ K. [d] Calculated molar absorption coefficient of **11·L** at the maximum of the corresponding B transition wavelength shown in parentheses (see Experimental Section). The standard deviations are listed in Table S1 (see Supporting Information). [e] Experimentally observed molar absorption coefficient of **11·L** at the maximum of the corresponding B transition wavelength shown in parentheses at the saturated amine concentration[7a] (the ϵ_{exp} values for **11·2$_R$** and**11·3$_S$** are remeasured).

11 resulting in an enhancement in the host−guest affinity and subsequently about a 2-fold increase of the K_m value in comparison to that of **4**. Interestingly, the cyclohexyl-containing **3** exhibits the strongest binding ability ($K_m = 7700-7800$ M^{-1}) among the amines used, while its pK_a value is almost the same as that of **2** which exhibits a moderate binding strength ($K_m = 3200-3500$ M^{-1}). Although the nature of this effect is not completely understood, it is likely that the CH−π interactions

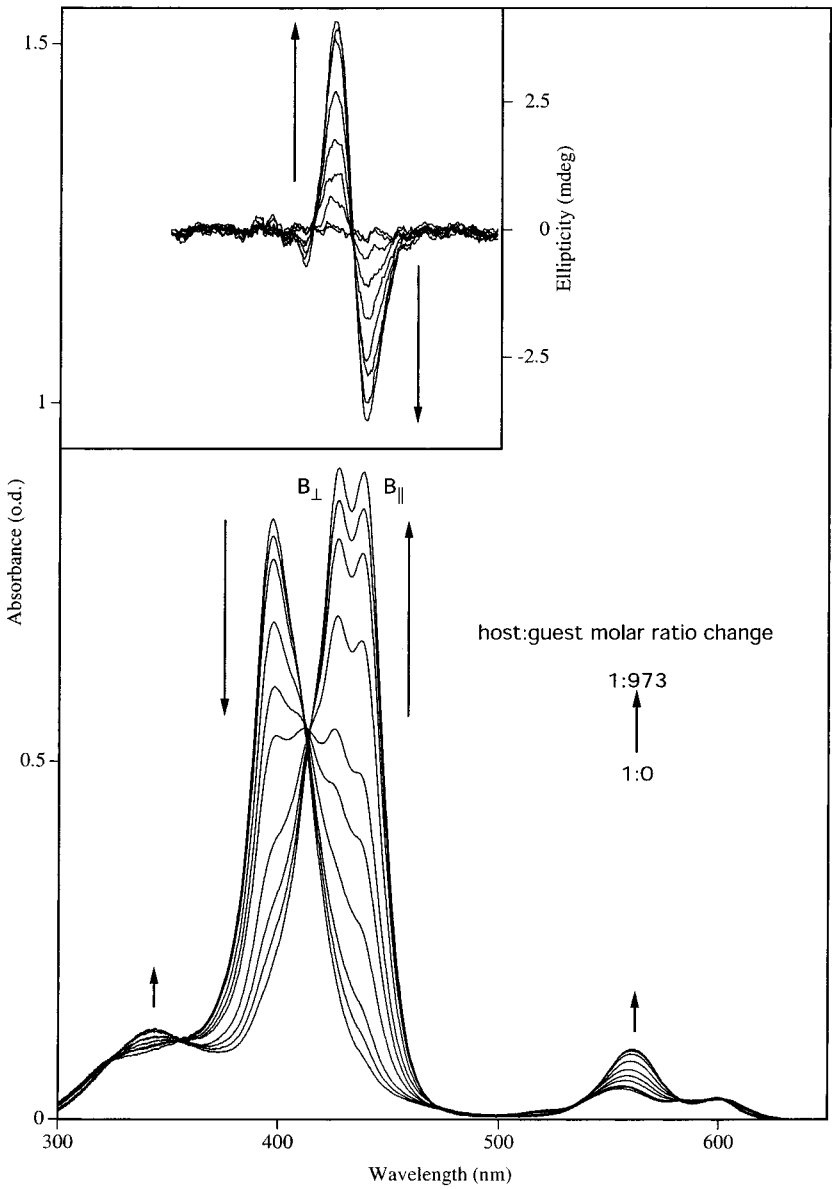

Figure 4. UV−vis and CD (inset) spectral changes of **1** ($C = 3.8 \times 10^{-6}$ M) in CH_2Cl_2 upon addition of $\mathbf{3_R}$ as the host:guest molar ratio changes from 1:0 to 1:973.

between cyclohexyl group and porphyrin macrocycle may contribute greatly to the stability of this complex. The positive role of this factor in the supramolecular association processes has been previously confirmed and thoroughly investigated.[3e,4i]

Hence, our results on complexation behavior of monomeric **11** with the chiral amines **2**−**5** are in a good agreement with the reported literature data and show clearly the formation of the 1:1 host−guest associates, the stability of which are strongly dependent on the ligand structure.

3. Guest Binding to the Bis-Porphyrin Host 1 as Determined by UV−Vis and CD Spectroscopy. Taking into account the interactions between monomeric metalloporphyrin and chiral ligands, we studied the complexation behavior of the bis-porphyrin host **1** in the presence of enantiopure guests with corresponding binding parameters obtained by means of various spectral methods. Since UV−vis spectroscopy has been applied to study the ligation process of the monomeric host **11**, the binding experiments carried out by optical spectral methods (UV−vis and CD) are examined first.

3.1. UV−Vis and CD Spectral Changes. Stepwise addition of **2**−**8** to **1** produces dramatic transformations in the UV−vis and CD spectra which finally become identical to those at the amine-saturated conditions.[7a] The representative spectral changes are shown in Figure 4. Thus, in the UV−vis spectra the intensity of the B band at 397 nm progressively decreases upon increase of the ligand molar excess from 1:0 to 1:973 (in the case of $\mathbf{3_R}$), and a new bathochromically shifted, well-resolved, and split Soret band with maxima at 425−427 nm ($B_\perp$ transition) and 436−438 nm ($B_\parallel$ transition) appears. The changes in the low-energy Q transition region (560−600 nm) are less pronounced and consist of substantial enhancement of the Q_{X01} transition intensity in comparison to almost no change in the Q_{X00} transition. Also there is the appearance and gradual increase of a high-energy transition at 344 nm.[16] These spectral changes

(16) In addition to the listed UV−vis spectral changes, there are the appearance and enhancement of another intense absorption at the high-energy region of the spectra (<340 nm) (upon addition of **5**) associated with the absorption of the naphthyl substituent.

are similar for all the amines used regardless of their structure and are associated with the described *syn*−*anti* conformational switching in **1** for the chiral[7] and achiral guests.[10] Furthermore, these observations are in full agreement with Kasha's exciton coupling theory[17] and with reported data for various bis- and multiporphyrin systems.[18]

In the CD spectra there is the appearance of a bisignate CD signal consisting of two major Cotton effects of opposite sign that gradually enhance as the amine concentration increases (Figure 4, inset). The positions of the first and second Cotton effects coincide very closely with the maxima of the split B bands in the UV−vis spectra, indicating that their origin is the same. The intensity and sign of the induced CD couplet is dependent upon the guest structure and absolute configuration, respectively. The detailed mechanism and controlling factors of the optical activity in **1** generated by various chiral guests were previously discussed in detail.[7]

3.2. Definition of the Binding Parameters According to Method A. The UV−vis spectral changes are followed at the wavelength corresponding to the maximum of the more bathochromically shifted B_{II} transition. This transition is chosen because the absorption of the final equilibrium species *anti*-**1**·$\mathbf{L}_2$ at this wavelength has the smallest overlapping with the absorptions of other equilibrium species,[19] and the difference between the optical densities at each titration step is the most prominent. In the case of CD spectroscopy as a monitoring parameter the total CD amplitude is chosen to reduce the influence of extraneous effects (such as the signal-to-noise ratio and any dissymmetry in the intensity of the Cotton effects induced by corresponding (*R*)- and (*S*)-enantiomers[7a]).[20] A representative plot of the UV−vis and CD monitoring parameters versus the molar excess of $\mathbf{3_R}$ is shown in Figure 5. There is a good coincidence of the UV−vis and CD experimental points with the exception of the early part of the plot (up to 1:170 ligand molar excess), where some deviations are observed. Interestingly, both the UV−vis and CD plots (as well as the other plots for the different systems studied) exhibit a clearly sigmoidal profile with saturation at the high ligand molar excess region, indicating unambiguously the cooperative nature of the complexation process between the external enantiopure ligands and **1**, leading to supramolecular chirality induction. This positive cooperativity (when the succeeding binding process is stronger than the preceding binding process) is observed in supramolecular chirogenesis in various systems. For example, it has been reported for binding of a resorcinol cyclic tetramer with glucopyranosides,[3f] binding by bis-porphyrins of oligosaccharides[4f] and chiral dicarboxylic acids,[4h] porphyrin assemblies on DNA,[21a] hydrogen bonding in helical self-assembled polymers,[21b] complexation of an optically active dicarboxylic acid with amines,[21c] DNA-templated formation of a helical cyanine dye J-aggregate.[21d]

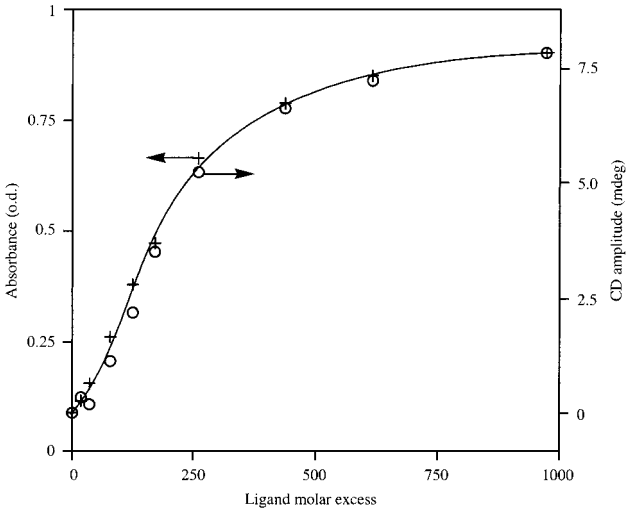

Figure 5. Dependencies of the UV−vis absorbance, monitored at 438 nm (B_{II} transition, crosses) and the total CD amplitude (circles) of **1** upon the molar excess of $\mathbf{3_R}$. The solid line represents the best theoretical fit for the 1:2 host−guest complexation process (see Experimental Section).

As previously stated,[7,10] supramolecular chirogenesis in **1** involves three major equilibrium steps: the first ligation (K_1), resulting in the formation of the monoligated *syn* species, *syn*-**1**·**L**; *syn*−*anti* conformational switching (K_S), giving the monoligated *anti* form, *anti*-**1**·**L**; and the second ligation (K_2), yielding the bis-ligated species *anti*-**1**·$\mathbf{L}_2$ (Figure 1). Relying on these equilibria, existing literature data and general binding principles, several reasonable assumptions can be made. First, since there are two equivalent binding sites in *syn*-**1**, and in *anti*-**1**·**L** the remaining ligand-free Zn porphyrin moiety should exhibit binding properties very similar to those of the monomeric zinc porphyrin **11**, with the K_2 value more resembling the K_m value, with the aforementioned dependencies on the ligand structure. Second, the K_1 value should be smaller than the K_2 value due to the positive cooperative character of the complexation process. Third, the K_S value is likely to be relatively small and independent of the ligand structure. Taking into account these considerations, a preliminary optimization is done. Thus, both the UV−vis and CD experimental points are well-fitted initially to the same set of theoretical equations for the simpler two-step complexation model using the nonlinear least-squares optimization[22] (see equilibria 2 and 3 in the Experimental Section). This model contains only two steps of the total equilibrium shown in Figure 1: the combined first ligand binding and *syn*−*anti* conformational switching (K_1') giving *anti*-**1**·**L** and the subsequent second ligation (K_2) producing *anti*-**1**·$\mathbf{L}_2$. The optimization allows determination of the K_1' and K_2 values. As expected for the cooperative binding, the latter is markedly larger than the former (K_2 values are listed in Table

(17) Kasha, M.; Rawls, H. R.; El-Bayoumi, M. A. *Pure Appl. Chem.* **1965**, *11*, 371.

(18) (a) Arnold, D. P. *Synlett* **1999**, 296. (b) Anderson, H. L. *Chem. Commun.* **1999**, 2323. (c) Kuciauskas, D.; Liddell, P. A.; Lin, S.; Johnson, T. E.; Weghorn, S. J.; Lindsey, J. S.; Moore, A. L.; Moore, T. A.; Gust, D. *J. Am. Chem. Soc.* **1999**, *121*, 8604. (d) Ruhlmann, L.; Lobstein, S.; Gross, M.; Giraudeau, A. *J. Org. Chem.* **1999**, *64*, 1352. (e) Ogawa, T.; Nishimoto, Y.; Yoshida, N.; Ono, N.; Osuka, A. *Angew. Chem., Int. Ed.* **1999**, *38*, 176. (f) Ponomarev, G. V.; Yashunsky, D. V.; Borovkov, V. V.; Sakata, Y.; Arnold, D. *Russ. Chem. Heterocycl. Cmpd.* **1997**, 1627. References 18g−z are in Supporting Information.

(19) The absorption maxima of the B transitions of other equilibrium species *syn*-**1**, *syn*-**1**·**L**, and *anti*-**1**·**L** should be more hypsochromically shifted in comparison to that of *anti*-**1**·$\mathbf{L}_2$ according to exciton coupling theory[17] (as for the difference between the *syn* and *anti* species) and coordination-induced bathochromic shifts of the metalloporphyrins[12,13] (as for the difference between *anti*-**1**·**L** and *anti*-**1**·$\mathbf{L}_2$). This was also proved by the calculation of the UV−vis spectrum of *anti*-**1**·**L** (see section 3.3).

(20) For amines **2** and **7** CD spectroscopy could not be applied for the titration experiments due to the very weak induced CD signal in **1** (Table 2).

(21) (a) Pasternack, R. F.; Bustamante, C.; Collings, P. J.; Giannetto, A.; Gibbs, E. J. *J. Am. Chem. Soc.* **1993**, *115*, 5393. (b) Hirschberg, J. H. K. K.; Brunsveld, L.; Ramzi, A.; Vekemans, J. A. J. M.; Sijbesma, R. P.; Meijer, E. W. *Nature* **2000**, *407*, 167. (c) Matsui, H.; Kushi, S.; Matsumoto, S.; Akazome, M.; Ogura, K. *Bull. Chem. Soc. Jpn.* **2000**, *73*, 991. (d) Wang, M.; Silva, G. L.; Armitage, B. A. *J. Am. Chem. Soc.* **2000**, *122*, 9977.

(22) A 1:1 equilibrium model resulted in very poor data fits.

Table 2. Binding, UV−Vis and CD Spectral Data of the System **1**·$\mathbf{L}_2$ with Different Chiral Amines[a]

system	binding constants[b] K_1 (M^{-1})	K_s	K_2 (M^{-1})	Gibbs free energy $\Delta G°$ at 293 K[c] (kcal mol^{-1})	calculated UV–vis data ϵ_{calc}[d] (10^5 (M^{-1} cm^{-1})) [λ_{max} (nm)]	observed UV–vis data ϵ_{exp}[e] (10^5 (M^{-1} cm^{-1})) [λ_{max} (nm)]	calculated CD data A_{calc}[f] (M^{-1} cm^{-1})	observed CD data A_{exp}[g] (M^{-1} cm^{-1})
1·$(\mathbf{2_R})_2$[h]	56	3.4	2900	−7.7	2.03 [437]	2.18 [437]	−	−20.5
1·$(\mathbf{2_S})_2$[h]	63	3.9	3100	−7.9	2.16 [437]	2.17 [437]	−	+18.0
1·$(\mathbf{3_R})_2$	47	3.8	10600	−8.4	2.40 [438]	2.53 [438]	−66	−72.7
1·$(\mathbf{3_S})_2$	46	3.8	10600	−8.4	2.39 [438]	2.46 [438]	+62	+67.8
1·$(\mathbf{4_R})_2$	27	4.0	1000	−6.7	1.79 [436]	2.11 [436]	−91	−84.1
1·$(\mathbf{4_S})_2$	27	3.8	1000	−6.7	2.04 [436]	2.12 [436]	+76	+78.4
1·$(\mathbf{5_R})_2$	48	3.9	2500	−7.6	1.85 [436]	2.12 [436]	−127	−107.9
1·$(\mathbf{5_S})_2$	48	3.9	2500	−7.6	2.10 [436]	2.14 [436]	+109	+107.7
1·$(\mathbf{6_S})_2$	83	4.0	4500	−8.3	2.08 [437]	2.54 [437]	+121	+129.7
1·$(\mathbf{7_S})_2$[h]	78	3.9	3700	−8.1	2.37 [437]	2.41 [437]	−	+11.9
1·$(\mathbf{8_R})_2$	11	3.1	410	−5.6	2.54 [437]	2.61 [437]	−106	−106.2
1·$(\mathbf{8_S})_2$	11	3.0	470	−5.6	2.46 [437]	2.49 [437]	+103	+107.7

[a] $C_1 = (2.9-3.8) \times 10^{-6}$ M in CH_2Cl_2. [b] The standard deviations are less than 5%. [c] $\Delta G° = -RT \ln(K_1K_sK_2)$, where $T = 293$ K. [d] Calculated molar absorption coefficient of **1**·$\mathbf{L}_2$ at the maximum of the corresponding B_{II} transition wavelength shown in parentheses (see Experimental Section). The standard deviations are listed in Table S1 (see Supporting Information). [e] Observed molar absorption coefficient of **1**·$\mathbf{L}_2$ at the maximum of the corresponding B_{II} transition wavelength shown in parentheses at the saturated amine concentration.[7a] [f] Calculated total amplitude of the CD couplets: $A_{calc} = \Delta\epsilon_{1calc} - \Delta\epsilon_{2calc}$ (see Experimental Section). The standard deviations are listed in Table S1 (see Supporting Information). [g] Total amplitude of the experimentally observed CD couplets at the saturated amine concentration: $A_{exp} = \Delta\epsilon_{1exp} - \Delta\epsilon_{2exp}$ (see ref 7a). [h] For these systems the binding constants are calculated on the basis of the UV−vis titration experiments only.

2, while K_1' values are not shown but can be easily calculated as described in the Experimental Section and below). Furthermore, as predicted, the K_2 values are of the same order of magnitude as the K_m values and follow the same tendencies of the ligand structural dependencies: aliphatic amines are more effectively bound to the host than aromatic amines, and ligands with an expanded aromatic system exhibit enhancement of the host−guest affinity. Additionally, it was shown that the secondary amines **8** have K_2 values about two times smaller than those of the primary amines **4**.

Further analysis of the complexation isotherm in order to obtain equilibrium parameters of the two initial steps (K_1 and K_S) of the supramolecular chirogenesis in **1** (Figure 1) is done as follows. The K_2 values are fixed and the equilibrium 2 which contains the two above-mentioned processes is divided into two individual equilibria: first ligation (K_1) and *syn*−*anti* conformational switching (K_S) taking into account that $K_1' = K_1K_S$ and that K_S is relatively small and independent of the ligand structure (see equilibria 4 and 5 in the Experimental Section). By this means, the K_1 and K_S values are obtained and shown in Table 2. As expected, the K_S values are essentially the same, regardless of the amine used, and small in comparison to the K_1 and K_2 values, indicating almost equal energy levels of the *syn*-**1**·**L** and *anti*-**1**·**L** species. The K_1 values are within the range of 27−83 M^{-1} for primary amines, which correlate closely with the binding energy of the first ligation process obtained by ab initio calculations.[11]

The calculated $\Delta G°$ values of the chirogenesis process in **1** are shown in Table 2 and vary from −6.7 to −8.4 kcal mol^{-1} for primary amines. If the zinc porphyrin subunits in **1** do not interact with each other, it is reasonable to expect that the $\Delta G°$ values of **1** would be two times greater than those of monomeric **11** upon binding with the same external ligand. However, the difference between the $\Delta G°$ values of **1** and monomeric **11** is within the range of −2.3 to −3.2 kcal mol^{-1} for the same amines, which is 1.7−2.1 kcal mol^{-1} more positive than the doubled $\Delta G°$ values of **11**. This points clearly to the presence of strong intramolecular interactions between two porphyrins in *syn*-**1** which are broken upon the competitive first ligation step.[11]

On the basis of the curve-fitting procedure the calculated ϵ_{calc} values of the B_{II} transitions and A_{calc} values of the induced CD couplets are in a good agreement with the experimentally observed UV−vis and CD data (Table 2), indicating that the described evaluation method is well-suited for analyzing multistep equilibria of the supramolecular chirogenesis in **1**.

3.3. Definition of the Binding Parameters According to Method B. To gain additional support for the equilibrium analysis discussed above (see section 3.2) and to obtain the spectral characteristics of the intermediate species, a nonlinear least-squares method developed for a multicomponent equilibrium system[9] which monitors a wide wavelength range[23] is applied for evaluation of the chirogenesis equilibria in **1**.

In the beginning, all three probable equilibria models are assumed: 1:1 host−guest complexation only according to equilibrium 2 (*model 1*); simultaneous 1:2 host−guest complexation according to equilibrium 6 (*model 2*); and stepwise 1:2 host−guest complexation according to the equilibria 2 and 3 (*model 3*), as shown in the Experimental Section and described in detail in section 3.2. The optimization procedure in accordance with these models is done for the UV−vis and CD spectral titration data of **1** with **5** resulting in the corresponding K_1', K_1'', and K_2 values (Table 3). The root-mean-square deviations are found to have the smallest values in the case of the equilibrium *model 3* for (*R*)- and for (*S*)-amines, as well as for both spectral methods, indicating that this equilibrium model is the most reliable. This is also in good agreement with the equilibrium mechanism described previously (see section 3.2). Furthermore, the $\Delta G°$ values obtained by method B (see Table 3) correlate well with those obtained by method A (see Table 2) for the same amines.

Method B has the additional advantage that it is possible to evaluate not only the spectrum of the final product, but also the spectrum of the intermediate species involved in the equilibrium process over the wavelength range studied. Using this option, the UV−vis and CD spectral profiles of *anti*-**1**·$\mathbf{5_R}$ and *anti*-**1**·$(\mathbf{5_R})_2$ are calculated (Figure 6). The calculated UV−

(23) The wavelength region of the most intense porphyrin B bands is used for the analysis of the UV−vis and CD spectral data.

Table 3. Calculated Data of Binding of $\mathbf{5_R}$ and $\mathbf{5_S}$ Obtained According to the Different Equilibria Models

ligand	spectral method	equilibria model	binding constants[a] K_1 (M^{-1}) and K_1'' (M^{-2})	K_1' (M^{-1})	K_2 (M^{-1})	Gibbs free energy $\Delta G°$ at 293 K[b] (kcal mol^{-1})	rmsd[c]
$\mathbf{5_R}$	UV−vis	1	699	−	−	−3.9	0.0122
		2	575000	−	−	−7.7	0.0078
		3	−	388	1036	−7.6	0.0017
	CD	1	470	−	−	−3.6	0.2394
		2	430000	−	−	−7.6	0.1795
		3	−	591	1369	−8.1	0.1102
$\mathbf{5_S}$	UV−vis	1	665	−	−	−3.8	0.0132
		2	516000	−	−	−7.7	0.0062
		3	−	264	1268	−7.5	0.0020
	CD	1	437	−	−	−3.6	0.2160
		2	374000	−	−	−7.5	0.1216
		3	−	182	2565	−7.7	0.0951

[a] The standard deviations are listed in Table S1 (see Supporting Information). [b] $\Delta G° = -RT \ln(K_1')$, $\Delta G° = -RT \ln(K_1'')$, or $\Delta G° = -RT \ln(K_1'K_2)$, where $T = 293$ K. [c] Root-mean-square deviation.

vis and CD spectra of *anti*-**1**·$(\mathbf{5_R})_2$ and the corresponding spectra obtained experimentally at the saturated amine concentration conditions[7a] are well matched, clearly demonstrating the suitability of this method for the evaluation of the spectral properties of the equilibria species. In the case of *anti*-**1**·$\mathbf{5_R}$ the calculated B band (428 nm) is not split and is hypsochromically shifted in comparison to that of *anti*-**1**·$(\mathbf{5_R})_2$ which, as described above, is split into two components (426 nm for $B_\perp$ transition and 436 nm for $B_{||}$ transition). This is apparently because of the lack of the second ligand in the case of the *anti*-**1**·**L** species.[19] Indeed, similar tendencies have been observed upon examination of the UV−vis spectra of the *anti* form of the monoligated free base porphyrin−zinc porphyrin heterodimer and *anti*-**1**·$\mathbf{L}_2$.[10b] Reflecting these differences in the UV−vis spectra, the calculated CD couplet of *anti*-**1**·$\mathbf{5_R}$ is also hypsochromically shifted in comparison to that of *anti*-**1**·$(\mathbf{5_R})_2$ by 12 nm (as for the first Cotton effect). Also, the calculated total amplitude of the CD couplet of *anti*-**1**·$\mathbf{5_R}$ is 3.3 times smaller than that of *anti*-**1**·$(\mathbf{5_R})_2$ showing that the major contribution to the optical activity of monoligated *anti*-**1**·$\mathbf{5_R}$ is the point chirality induction effect studied previously for monomeric **11**·**L**,[7a] rather than supramolecular chirogenesis.

Additionally, this evaluation method also allowed the calculation of the dependency of the relative population of each equilibria species upon increase of the ligand concentration (Figure 7). The curve of the *anti*-**1**·$\mathbf{L}_2$ population shows a sigmoidal profile with a saturation behavior that reaches 86%

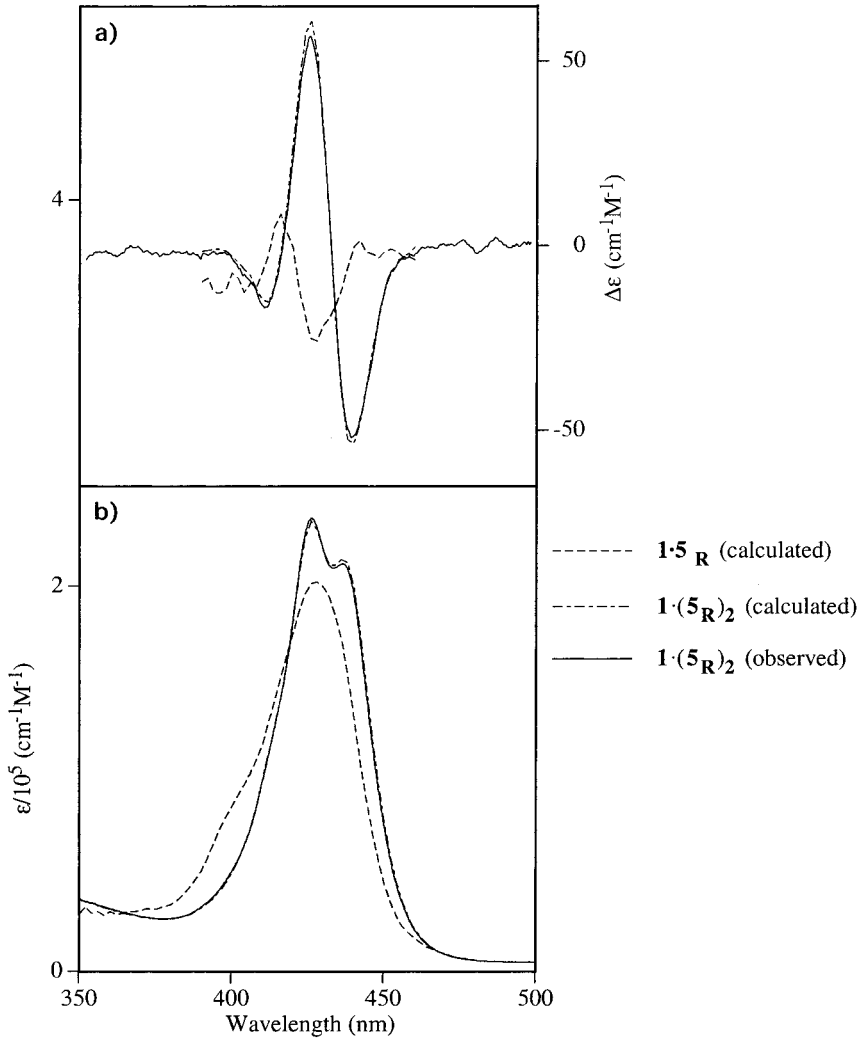

Figure 6. Calculated according to equilibrium *model 3* and experimentally observed at the saturated amine concentration conditions[7a] CD (a) and UV−vis (b) spectra of **1** in the presence of $\mathbf{5_R}$.

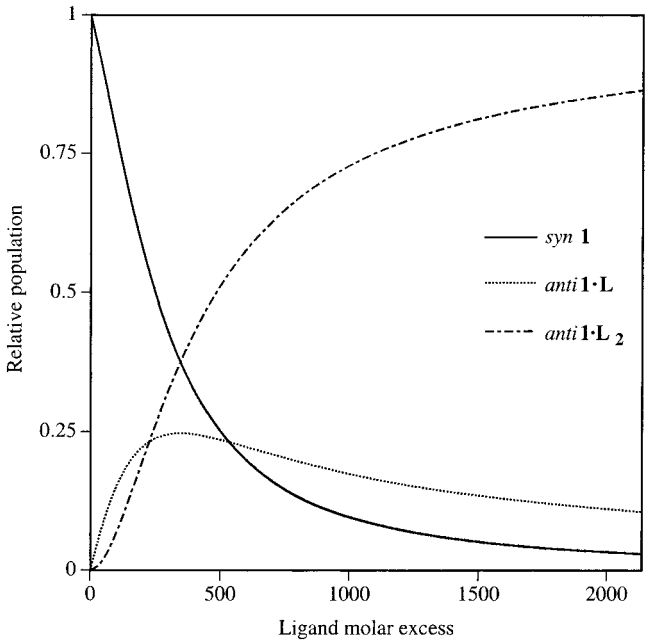

Figure 7. Dependence of the relative population of the *syn*-**1**, *anti*-**1·L** and *anti*-**1·L**$_2$ species calculated according to equilibrium *model 3* upon the molar excess of $\mathbf{5_R}$ based on the UV−vis titration data.

at 1:2000 ligand molar excess. The profile of the *anti*-**1·L** population exhibits initially a sharp rise, reaches a maximum (25%) at the 1:350 ligand molar excess and then decreases steadily down to 11% at the 1:2000 ligand molar excess. The population of the initial *syn*-**1** species drops in an exponential-like manner to 3% at the 1:2000 ligand molar excess.

3.4. Definition of the Thermodynamic Parameters by VT Optical Spectroscopic Methods. To obtain a comprehensive picture of the supramolecular chirogenesis in **1** the thermodynamic parameters of this process should be evaluated. For this purpose, VT UV−vis and CD experiments were carried out. Furthermore, VT spectroscopy is a necessary tool for studying the chirality induction processes involving alcohol ligands since these hydroxyl-containing compounds are known to have a weaker affinity for zinc porphyrins at room temperature in comparison to amines.[7c,10b]

The temperature-induced changes in UV−vis and CD spectra of the chiral ligand containing systems have been reported previously for chiral amines, alcohols,[7c] and achiral alcohols (UV−vis only).[10] These changes are indeed the same as those observed during the titration experiments described above (Figure 4) and include the appearance and gradual enhancement of the bathochromically shifted, split B band in the UV−vis spectra and the corresponding CD couplet upon lowering the temperature from 293 to 183 K (see Figure S1 in Supporting Information).

The spectral parameters monitored for the VT experiments were chosen to be the same as those in the case of the titration experiments: the absorption at the wavelength corresponding to the maximum of the B_{II} transition in the case of the UV−vis measurements and the total CD amplitude in the case of the CD measurements. The UV−vis and CD monitoring parameters are plotted versus temperature and the resulting dependencies shown in Figure 8. The progressive UV−vis changes exhibit a sigmoidal profile with saturation behavior at low temperatures, and fit well to the set of theoretical equations for the total

Table 4. Thermodynamic Parameters and Calculated UV−Vis Spectral Data of the System **1·L**$_2$ with Different Chiral Ligands[a]

	thermodynamic parameters			calculated UV–vis data
system	$\Delta H°$[b] (kcal mol^{-1})	$\Delta S°$[b] (cal mol^{-1} K^{-1})	$\Delta G°$ at 293 K[c] (kcal mol^{-1})	ϵ_{calc}[d] (10^5 (M^{-1} cm^{-1})) [λ_{max} (nm)]
1·(2$_R$)$_2$	−12.6	−15.6	−8.0	2.44 [436]
1·(3$_R$)$_2$	−14.3	−17.6	−9.1	2.11 [437]
1·(4$_R$)$_2$	−13.9	−22.2	−7.4	2.38 [436]
1·(4$_S$)$_2$	−14.3	−23.9	−7.3	2.31 [436]
1·(5$_R$)$_2$	−15.2	−24.6	−8.0	2.44 [436]
1·(5$_S$)$_2$	−16.8	−30.5	−7.9	2.34 [436]
1·(9$_R$)$_2$	−8.1	−29.6	0.6	2.57 [432]
1·(10$_R$)$_2$	−7.9	−29.6	0.8	1.95 [431]
1·(10$_S$)$_2$	−7.8	−29.6	0.9	2.32 [431]

[a] $C_{\mathbf{1}} = (3.3-3.9) \times 10^{-6}$ M, $C_{\mathbf{2-5}} = (1.4-4.0) \times 10^{-4}$ M, $C_{\mathbf{9,10}} = (3.3-3.9) \times 10^{-1}$ M in CH_2Cl_2. [b] Obtained from a van't Hoff-type analysis (see Experimental Section). The standard deviations are listed in Table S1 (see Supporting Information). [c] $\Delta G° = \Delta H° - T\Delta S°$, where $T = 293$ K. [d] Calculated molar absorption coefficient of **1·L**$_2$ at the maximum of the corresponding B_{II} transition wavelength shown in parentheses (see Experimental Section). The standard deviations are listed in Table S1 (see Supporting Information).

equilibrium 6 using the nonlinear least-squares optimization procedure according to the van't Hoff type analysis (see Experimental Section). This approach was successfully used previously for evaluation of the *syn*−*anti* conformational switching in **1** induced by achiral alcohols.[10b] In the case of chiral ligands it also allows us to determine the corresponding thermodynamic parameters ($\Delta H°$, $\Delta S°$, and $\Delta G°$) and ϵ_{calc} values for the supramolecular chirogenesis process in the various systems studied (Table 4). Thus, the $\Delta H°$ and $\Delta S°$ values of the alcohol containing systems (**1·(9)**$_2$ and **1·(10)**$_2$) are within the same range as those for the systems containing achiral alcohols.[10b] The $\Delta S°$ values for the alcohol- and amine-containing systems studied vary from −15.6 to −30.5 kcal mol^{-1} K^{-1} and are almost independent of the ligand binding group, while the $\Delta H°$ values are strongly affected by this factor. This indicates that there is no clear entalpy−entropy compensation between the two classes of ligands. The $\Delta H°$ values of **1·(9)**$_2$ and **1·(10)**$_2$ vary from −7.8 to −8.1 kcal mol^{-1} and are less negative in comparison to those of the amine-containing systems (**1·(2)**$_2$ to **1·(5)**$_2$), which are in the range of −12.6 to −16.8 kcal mol^{-1}. Since all the complexations are enthalpically driven, this difference between the $\Delta H°$ values (and the independence to the ΔS values) correlates with the well-known, and above-mentioned fact, that amines have greater affinity for zinc porphyrins than the corresponding alcohols. The calculated $\Delta G°$ values of **1·(9)**$_2$ and **1·(10)**$_2$ are positive at 293 K, making the complexation process and, as a consequence, the chirogenesis phenomenon thermodynamically unfavorable. On the other hand, decreasing the temperature leads to a significant decrease in the total free energy change, resulting in negative $\Delta G°$ values, and hence shifting the equilibrium toward the chiral *anti*-**1·L**$_2$ form. The $\Delta G°$ values of **1·(2)**$_2$ to **1·(5)**$_2$ are negative and practically the same as those derived from the titration experiments discussed above (see Tables 2 and 3), indicating that the amine complexation is thermodynamically favorable at room temperature, which subsequently leads to generating chirality induction in **1**. The calculated ϵ_{calc} values compare well with those obtained from the titration experiments (Table 2), experimental measurements at saturated amine concentration,[7a] and thermodynamic analysis of the achiral alcohol-containing systems.[10b]

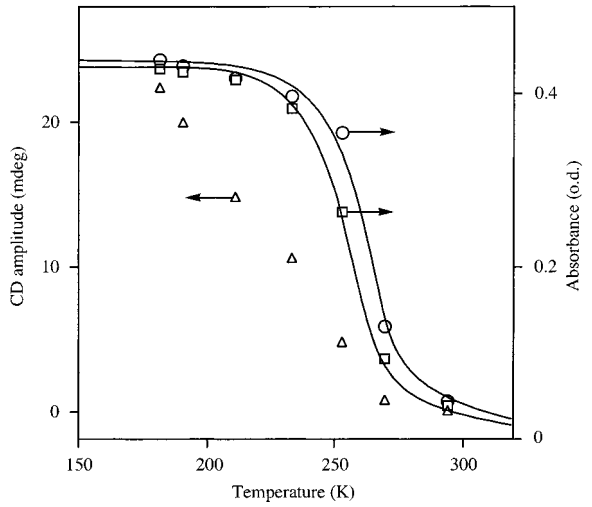

Figure 8. Temperature dependencies of the UV−vis absorbance monitored at 436 nm (B_{II} transition) (squares and circles) and the total CD amplitude (triangles) of **1** in the presence of $\mathbf{4_R}$ (squares and triangles) and $\mathbf{5_R}$ (circles) at the low ligand molar excess region. The solid lines represent the best theoretical fits for the thermodynamic equilibrium of the 1:2 host−guest complexation process (see Experimental Section).

In the case of the CD amplitude change upon lowering the temperature, a very interesting and surprising phenomenon is observed. Thus, in contrast to the titration experiments (Figure 5), the CD temperature dependence does not coincide at all with the corresponding UV−vis temperature dependence. An example of this behavior is shown in Figure 8 for $\mathbf{4_R}$. The CD changes are delayed in comparison to the UV−vis changes, and unlike the UV−vis changes, do not show a saturation behavior within the temperature region studied. Although this discrepancy is not as yet fully understood, a straightforward and plausible origin of this phenomenon is as follows. Since this is a highly dynamic system with the spectral contribution of a number of different species, it is realized that while they may have similar contributions to the UV−vis spectra, some of the conformations are unable to generate supramolecular chirality in **1**,[7a] or only contribute weakly to the induced CD spectrum. This can be seen as follows. VT experiments were carried out with approximately a 40−120-fold ligand molar excess to monitor the whole range of the spectral changes over the temperatures used. The initial relative population of the equilibrium species at room temperature is fixed at about 74−92% of *syn*-**1**, 17−7% of *anti*-**1·L**, and 9−1% of *anti*-**1·L**$_2$ based on Figure 7. As one can see, the population of the intermediate *anti*-**1·L** species is relatively large, although its anisotropy factor ($g = \Delta\epsilon/\epsilon$) that controls the intensity of the CD signal is substantially smaller than that of *anti*-**1·L**$_2$ based on the calculated UV−vis and CD spectra (Figure 6). Hence, while the absorption intensities of the B bands of *anti*-**1·L** and *anti*-**1·L**$_2$ are fairly comparable, thus resulting in apparent UV−vis saturation at lower temperatures, the CD signal of *anti*-**1·L** is greatly reduced in comparison to that of *anti*-**1·L**$_2$. This may cause a lag of the VT CD changes in comparison to the VT UV−vis changes at these fixed host:guest ratios where the population of the *anti*-**1·L** species is sufficiently large.

4. Guest Binding to the Bis-Porphyrin Host 1 as Determined by ^{1}H NMR Spectroscopy. After detailed investigation of the ligand binding to **1** by optical spectroscopy, the methods of ^{1}H NMR spectroscopy can be applied to study further the host−guest interactions which play the major role in the process of supramolecular chirogenesis. Particularly, this approach makes it possible to analyze quantitatively this equilibrium at different concentration ranges.

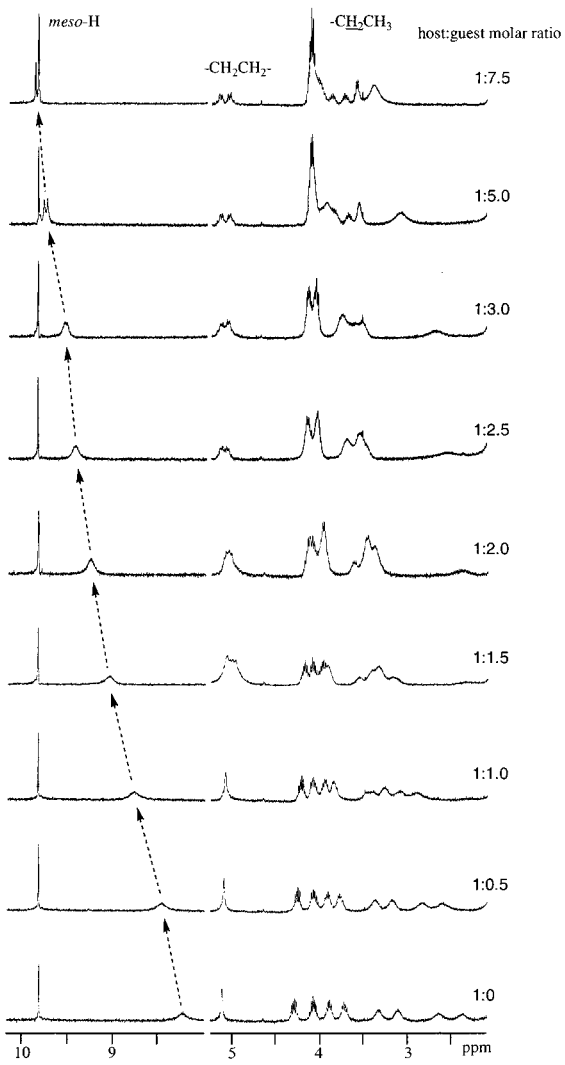

Figure 9. Selected areas of the ^{1}H NMR spectral changes of **1** ($C = 1.6 \times 10^{-3}$ M) in $CDCl_3$ upon addition of $\mathbf{4_R}$ at the host−guest molar ratio ranging from 1:0 to 1:7.5 at 273 K.

4.1. ^{1}H NMR Spectral Changes. The ^{1}H NMR titration experiments were carried out at 293 and 273 K since the monitored proton resonances in the recorded spectra are well-resolved and defined at these temperatures. Upon stepwise addition of chiral ligands to **1** the ^{1}H NMR spectral profile is profoundly transformed due to *syn*−*anti* conformational switching producing the resulting spectrum which is similar to that of the *anti* species reported previously.[7a,c,e] The general tendency of the ^{1}H NMR spectral changes is clearly seen in Figure 9 in the case of $\mathbf{4_R}$. The 10,20-*meso* protons are gradually shifted downfield, while the position of the 15-meso protons remains essentially unchanged. This is because the 10,20-*meso* protons are strongly shielded by the ring current effect of the neighboring porphyrin in *syn*-**1** and hence are the most affected by the deshielding process upon the conformational switching from *syn* to *anti* form. The eight well-resolved signals of the $-CH_2$-CH_3 protons transform into several broad multiplets which are located at a more downfield region due to increased equivalence

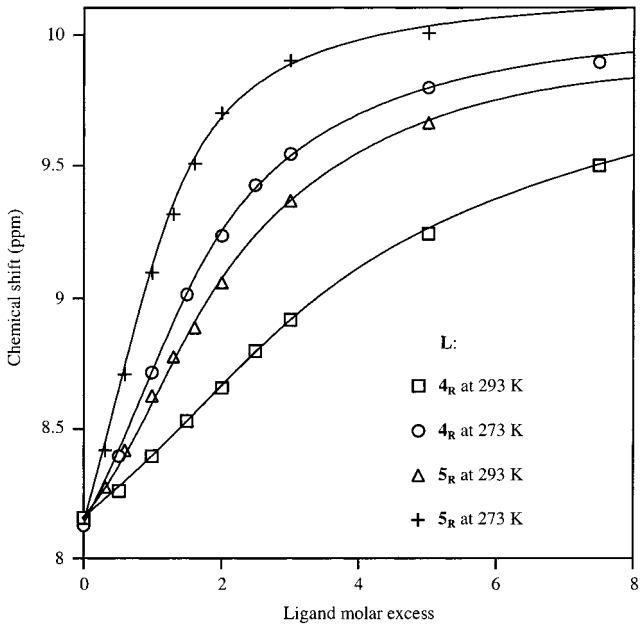

Figure 10. Dependency of the chemical shift of the 10,20-*meso* proton (which is the most downfield shifted) of **1** upon the molar excess of **L** (**4**$_R$ and **5**$_R$) at two temperatures (273 and 293 K). The solid lines represent the best theoretical fits for the 1:2 host−guest complexation process (see Experimental Section).

arising from their easier rotation in the *anti* form in comparison to the more rigid *syn* conformer. Similar spectral differences have been observed for the more structurally fixed cis and trans isomers of the ethylene-bridged bis-porphyrin.[24] It is important to note that in the case of addition of chiral aromatic amines the 10,20-*meso* protons and $-CH_2CH_2-$ protons are remarkably split into two signals of equal intensity. This proton nonequivalence is a result of the proton's different location with respect to the neighboring porphyrin ring in the screw structure of the *anti* form. All these changes are typical for the chirogenesis process in **1** induced by interaction with chiral ligands and has been recently studied in detail.[7a,c,e]

4.2. Definition of the Binding Parameters According to Method A. For analyzing the overall equilibrium of the chirogenesis process in **1**, the more downfield shifted resonance of the split 10- or 20-*meso* proton signals that depends on the screw direction in the corresponding *anti* form[7a,e] was chosen as a monitoring parameter. This is due to the fact that these protons are the most affected by the deshielding effect arising from the *syn*−*anti* conformational switching and subsequent formation of the chiral screw structure. Representative dependencies of the monitoring chemical shifts upon the ligand molar excess for several systems containing **4**$_R$ and **5**$_R$ at 293 and 273 K are shown in Figure 10. The plot profiles clearly exhibit a sigmoidal behavior, as observed in the case of the optical titration experiments (see section 3.2 and Figure 5), indicating a similar cooperative mechanism of ligand binding with **1** at the higher concentration range used for the ^{1}H NMR measurements (see footnote a in Table 5). The steepness of the plots reflects the overall ligand binding strength, with the relative steepness in the following order: **5**$_R$ at 273 K > **4**$_R$ at 273 K > **5**$_R$ at 293 K > **4**$_R$ at 293 K. This indicates that **5**$_R$ has a greater affinity to **1** than **4**$_R$ due to the expanded aromatic system, as discussed in Section 3.2, and lowering the temperature enhances the amine-binding strength toward zinc porphyrins.

Table 5. Binding and ^{1}H NMR Spectral Data of the System **1**·**L**$_2$ with Different Amines[a]

system	T (K)	binding constants[b] K_1 (M^{-1})	K_S	K_2 (M^{-1})	Gibbs free energy $\Delta G°$ at 293 K[c] (kcal mol^{-1})	calculated ^{1}H NMR data δ_{calc}[d] (ppm)	observed ^{1}H NMR data δ_{exp}[e] (ppm)
1·(**2**$_R$)$_2$	293	30	2.0	710	−6.2	10.15	
	273	45	2.3	1700	−6.6	10.16	
1·(**4**$_R$)$_2$	293	26	2.0	458	−5.9	10.16	10.03
	273	40	2.2	1297	−6.3	10.16	
1·(**4**$_S$)$_2$	293	27	2.0	489	−5.9	10.16	10.03
	273	42	2.2	1512	−6.4	10.16	
1·(**4**$_{RS}$)$_2$	293	25	1.9	437	−5.8	10.10	10.00
	273	38	2.2	1100	−6.2	10.12	
1·(**5**$_R$)$_2$	293	38	2.1	1188	−6.7	10.17	10.09
	273	51	2.4	3592	−7.0	10.17	

[a] $C_1 = (1.57-1.62) \times 10^{-3}$ M in $CDCl_3$. [b] The standard deviations are less than 5%. [c] $\Delta G° = -RT \ln(K_1K_SK_2)$, where T = 293 K or 273 K. [d] Calculated chemical shift for the most downfield shifted 10,20-*meso* proton of **1**·**L**$_2$ (see Experimental Section). The standard deviations are listed in Table S1 (see Supporting Information). [e] Experimentally observed chemical shift for the most downfield shifted 10,20-*meso* proton of **1**·**L**$_2$ at 213 K at the ligand molar excess of 5 (for **2** and **5**) and 7.5 (for **4**).

Applying the same Method A as described above (see Experimental Section and section 3.2) for analyzing the total supramolecular chirogenesis equilibria, an excellent fit of the ^{1}H NMR experimental data to the theoretical isotherm for the stepwise complexation model (equilibria 4, 5, and 3) is obtained by the nonlinear least-squares optimization (Figure 10). The corresponding binding parameters derived from the fitting procedure are summarized in Table 5. Although the K_1, K_S, and K_2 values obtained by ^{1}H NMR spectroscopy are smaller than the corresponding equilibrium constants obtained by optical spectroscopies as results of the higher concentrations in the former case (see footnotes a in Tables 5 and 2) and different solvents, the general tendencies in both cases are essentially the same. Thus, the K_S values are practically the same for the all amines used, regardless of their structure, and are the smallest in comparison to the K_1 and K_2 values. Reflecting the cooperative character of the ligand binding, the K_2 values are always greater than the K_1 values. The calculated $\Delta G°$ values of the total chirogenesis equilibrium are more positive (by 0.8−1.5 kcal mol^{-1}) than those obtained by optical spectroscopies (Table 2) due to the aforementioned concentration difference, while lowering the temperature markedly increases the magnitude of the $\Delta G°$ values because of enhancement of the ligand affinity. As an additional criterion of the quality of both the equilibrium model and fitting method, the calculated chemical shifts are compared with the experimentally found values. The δ_{calc} values are in the range of 10.10−10.17 ppm regardless of the temperature used. These data are in good agreement with the δ_{exp} values for the corresponding ligands observed at 231 K where the equilibrium is shifted almost entirely toward the *anti*-**1**·**L**$_2$ form. Furthermore, additional evidence of the credibility of the δ_{calc} values is obtained by comparison with the 10,20-*meso* proton chemical shift of the more conformationally stable trans isomer of the ethylene-bridged bis-porphyrin (δ_{trans}), which is in a fully extended form due to the structural rigidity provided by the double bond between the two porphyrin moieties.[18v] Thus, the δ_{trans} value is 10.12 ppm[25] which is in excellent agreement with the δ_{calc} values.

(24) Ponomarev, G. V.; Borovkov, V. V.; Sugiura, K.-i.; Sakata, Y.; Shul'ga, A. M. *Tetrahedron Lett.* **1993**, *34*, 2153.

Table 6. Thermodynamic Parameters and Calculated ^{1}H NMR Spectral Data of the System **1**·$\mathbf{L}_2$ with Different Amines[a]

system	thermodynamic parameters: $\Delta H°$[b] (kcal mol^{-1})	$\Delta S°$[b] (cal mol^{-1} K^{-1})	$\Delta G°$ at 293 K[c] (kcal mol^{-1})	calculated ^{1}H NMR data: δ_{calc}[d] (ppm)
1·$(\mathbf{2_R})_2$	−8.33	−5.9	−6.6	10.00
1·$(\mathbf{4_R})_2$	−9.95	−12.4	−6.3	10.04
1·$(\mathbf{4_S})_2$	−9.85	−11.8	−6.4	10.05
1·$(\mathbf{4_{RS}})_2$	−9.12	−10.1	−6.2	10.03
1·$(\mathbf{5_R})_2$	−11.09	−14.4	−6.9	10.10

[a] $C_\mathbf{1} = (1.57-1.62) \times 10^{-3}$ M, $C_\mathbf{L} = (3.14-3.24) \times 10^{-3}$ M in $CDCl_3$. [b] Obtained from a van't Hoff-type analysis (see Experimental Section). The standard deviations are listed in Table S1 (see Supporting Information). [c] $\Delta G° = \Delta H° - T\Delta S°$, where $T = 293$ K. [d] Calculated chemical shift for the most downfield shifted 10,20-*meso* proton of **1**·$\mathbf{L}_2$ (see Experimental Section). The standard deviations are listed in Table S1 (see Supporting Information).

4.3. Definition of the Thermodynamic Parameters by the VT ^{1}H NMR Method. As in the case of the optical spectroscopy approach, VT ^{1}H NMR experiments were carried out to determine the corresponding thermodynamic parameters of the chirogenesis process at higher concentration range.

To shift the total equilibrium from the initial *syn*-**1** at 293 K toward the *anti*-**1**·$\mathbf{L}_2$ species, a constant 1:2 host−guest molar ratio and temperature reduction were used as a controlling tool to follow the whole range of the conformational changes. Upon lowering the temperature, the same spectral transformations are observed as for the titration experiments (see Section 4.1), including downfield shifts of the 10,20-*meso* protons, splitting of the 10,20-*meso* and $-CH_2CH_2-$ protons and gradual changes of the eight multiplets of the $-C\underline{H}_2CH_3$ protons (an example for $\mathbf{4_R}$ is shown in Figure S2 of Supporting Information). Also, as in the case of the titration experiments, the same monitoring parameter (the more downfield-shifted resonance of the split 10- or 20-*meso* proton signals) was chosen for the VT measurements. Applying the standard fitting procedure according to the van't Hoff type analysis as described in the Experimental Section and in section 3.4, the corresponding thermodynamic parameters and calculated ^{1}H NMR data of the chirogenesis process are obtained (Table 6). Although the $\Delta H°$, $\Delta S°$, and $\Delta G°$ values are less negative than those determined by the VT UV−vis methods for the corresponding systems (see, Table 4) due to the higher concentration conditions, the general tendencies are also the same. Furthermore, the $\Delta G°$ and δ_{calc} values correlate well with those obtained by the titration experiments (and with the δ_{exp} values as well for the chemical shift comparison) for the same systems (see Table 5).

5. VT ESI MS Spectral Changes. As additional support for the existing equilibria mechanism of the supramolecular chirogenesis process in **1** induced by external chiral ligands, ESI MS experiments were carried out to detect the presence of all equilibrium species. The standard titration procedure at room temperature is not applicable in this particular case due to moderate binding constants, and as a consequence the large guest molar excess leads to increased noise level. Therefore, VT measurements with a fixed host−guest molar ratio were chosen as the most suitable approach and the same samples as used for the VT ^{1}H NMR experiments were applied to study the chirogenesis process by ESI MS. A representative example is shown in Figure 11 for $\mathbf{5_R}$. Thus, while in the spectrum of **1** there is only a signal associated with the corresponding molecular ion $[\mathbf{1}]^+$, addition of the 2 equiv of the external ligand results in appearance of a new peak attributed to formation of a 1:1 complex $[\mathbf{1}\cdot\mathbf{L}]^+$ at 110 °C. Lowering the temperature produces another signal corresponding to the molecular ion $[\mathbf{1}\cdot\mathbf{L}_2]^+$ due to enhancement of the ligand binding strength which has been observed by other spectroscopic techniques (see, sections 3.4 and 4.3). Further decrease of the temperature increases the $[\mathbf{1}\cdot\mathbf{L}_2]^+$ signal intensity. Although quantitative analysis is not possible in the case of the VT ESI MS measurements, qualitatively these results clearly show the presence of all three major species (**1**, **1**·**L**, and **1**·$\mathbf{L}_2$) participat

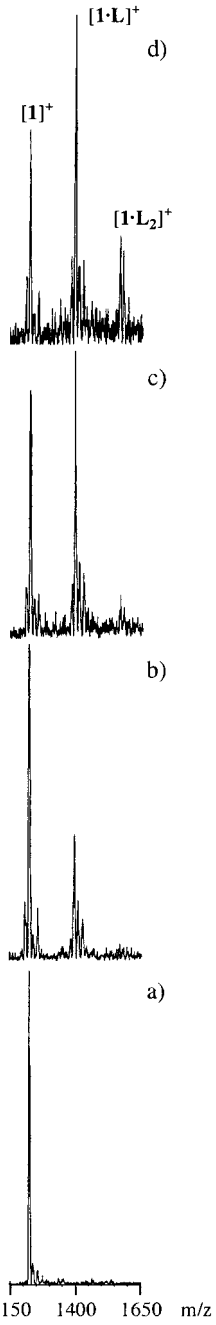

Figure 11. Selected areas of the ESI mass spectra of **1** in $CDCl_3$ without external ligand at 110 °C (a) and in the presence of $\mathbf{5_R}$ at 110 °C (b), 90 °C (c), and 70 °C (d).

(25) Shul'ga, A. M.; Ponomarev, G. V. *Russ. Chem. Heterocycl. Cmpd.* **1988**, 339.

ing in the total chirogenesis equilibrium and are in good agreement with the general tendencies observed during the VT experiments carried out by optical and ^{1}H NMR spectral methods.

Conclusions

This work clearly demonstrates the existence of a multistep equilibrium in the supramolecular chirogenesis process in the achiral host as induced by noncovalent interactions with chiral guests containing an amine/hydroxyl group which is able to coordinate to the central zinc ion of the porphyrin. It is proved that the total equilibrium includes three major steps: (1) ligand binding to the *syn* form of bis(zinc porphyrin) leading to destruction of the strong $\pi-\pi$ interporphyrin interactions, (2) induced *syn*−*anti* conformational switching producing the extended *anti* form, and (3), binding of a second ligand to the neighboring porphyrin moiety generating supramolecular chirality. All experimental data obtained by various spectroscopic methods agree well with this model. The quantitative analysis of the experimental titration and VT data using the standard least-squares fitting procedure reveals that the chirality induction is a highly cooperative process, since the second ligation is significantly stronger than the first ligation. The guest-binding strength is dependent upon the nature of the ligand substituents and corresponding functional groups, while the *syn*−*anti* conformational switching is independent of the guest structure and proceeds without appreciable free energy change. The general tendencies of the complexation process are as follows. Amines have greater affinity than alcohols; secondary amines bind more weakly than primary amines; aliphatic-containing ligands bind more strongly than aromatic-containing ligands; enlargement of the aromatic system increases the binding strength.

The results obtained offer a clearer view of the total mechanism of supramolecular chirogenesis in natural and artificial systems and may have practical implications in the design of chiroptical molecular devices. Specifically, a high chiroptical sensitivity of the host molecule to external guest molecules makes it possible to use this system as an effective chiral sensor even for alcohols which possess low affinity toward zinc porphyrins at room temperature by enhancing the alcohol binding strength upon lowering the temperature. Further studies to enhance the applicability and sensitivity of this system (particularly development of a room-temperature chiral sensor for alcohols, as well as for other types of chiral compounds) are currently in progress and will be the subject of future reports from our group.

Acknowledgment. We thank Mr. M. Abe for technical support with the ESI MS measurements and Dr. G. A. Hembury for assistance in the preparation of this manuscript.

Note Added after ASAP: There were errors in equations 2 and 3 in the version posted ASAP February 27, 2002; the corrected version was posted February 28, 2002.

Supporting Information Available: Additional references, standard deviations and VT UV−vis, CD, and ^{1}H NMR spectra (PDF). This material is available free of charge via the Internet at http://pubs.acs.org.

JA0172520